

Real time decoherence of Landau and Levitov quasi-particles in quantum Hall edge channels

D. Ferraro^{1,2,3}, B. Roussel¹, C. Cabart¹, E. Thibierge¹, G. Fève⁴, Ch. Grenier⁵, and P. Degiovanni¹

(1) *Université de Lyon, Fédération de Physique A.-M. Ampère, CNRS - Laboratoire de Physique de l'Ecole Normale Supérieure de Lyon, 46 Allée d'Italie, 69364 Lyon Cedex 07, France*

(2) *Aix Marseille Université, CNRS, CPT, UMR 7332, 13288 Marseille, France*

(3) *Université de Toulon, CNRS, CPT, UMR 7332, 83957 La Garde, France*

(4) *Laboratoire Pierre Aigrain, Ecole Normale Supérieure, CNRS, Université Pierre et Marie Curie, Université Denis Diderot, 24 rue Lhomond, 75231 Paris Cedex 05, France and*

(5) *Institute for Quantum Electronics, ETH Zurich, 8093 Zurich, Switzerland*

Quantum Hall edge channels at integer filling factor provide a unique test-bench to understand decoherence and relaxation of single electronic excitations in a ballistic quantum conductor. In this Letter, we obtain a full visualization of the decoherence scenario of energy (Landau) and time (Levitov) resolved single electron excitations at filling factor $\nu = 2$. We show that the Landau excitation exhibits a fast relaxation followed by spin-charge separation whereas the Levitov excitation only experiences spin-charge separation. We finally suggest to use Hong-Ou-Mandel type experiments to probe specific signatures of these different scenarios.

PACS numbers: 73.23.-b, 73.43.-f, 71.10.Pm, 73.43.Lp

The recent demonstration of on-demand single electron sources able to inject single electronic excitations into quantum Hall edge channels¹⁻³ or 2DEG^{4,5} has opened a new era of quantum coherent electronics. By combining these sources to electronic beam splitters, experiments analogous to the celebrated Hanbury-Brown and Twiss and Hong-Ou-Mandel⁶ experiments have been demonstrated at the single electron level^{7,8} thus opening the way to electron quantum optics^{9,10}. However, this emerging field goes beyond a simple analogy with photon quantum optics: first of all, the Fermi statistics of electrons differs from the Bose statistics of photons and leads to the Fermi sea, a state with no analogue in photon quantum optics. Moreover, electrically charged electrons experience Coulomb interactions which, despite screening, are expected to induce strong decoherence effects as demonstrated by Mach-Zehnder interferometry experiments¹¹⁻¹⁵. Moreover, an in-depth study of the relaxation of a non-equilibrium electronic distribution at filling factor $\nu = 2$ has shown that a description of the quantum Hall edge channels in terms of Landau quasi-particle excitations is not valid^{16,17}.

Although the above results on single electron relaxation and decoherence have been obtained by considering stationary sources and time averaged quantities such as the electron distribution function, the recent demonstration of the electronic Hong-Ou-Mandel (HOM) experiment⁸ calls for a time resolved approach to single electron coherence taking into account the finite duration of the electronic excitation. The aim of this Letter is precisely to discuss the decoherence scenario of two single electron excitations emitted by state of the art sources. First, the Landau quasi-particles correspond to a Lorentzian wave packet in energy emitted by a properly operated quantum dot¹. Secondly, the Levitov quasi-particles or Levitons⁴

are the minimal single electron state obtained by applying a Lorentzian time-dependent potential with quantized flux¹⁸. We show that comparing the real time aspects of their decoherence brings a better understanding of the underlying mechanisms of electronic decoherence whose specific features could be experimentally tested in HOM experiments.

Recently, finite frequency admittance measurements have demonstrated the existence of collective neutral and charged modes of the $\nu = 2$ quantum Hall edge channel system¹⁹. At low energy, this experiment has validated the physical picture of two non dispersive eigenmodes emerging from strong inter-channel effective Coulomb interactions: the fast mode carries the total charge whereas the slow one is neutral (dipolar) and therefore, in spin polarized channels, is expected to carry only spin. The existence of these two modes leads to the well known image of spin-charge separation²⁰ clearly valid for collective excitations generated by a time dependent voltage pulse²¹ such as the Levitons⁴.

But is this simple image still valid when considering an arbitrary single electron excitation? In particular, can spin-charge separation be observed for an energy resolved single electron excitation? Looking at the time dependent average current, the answer is certainly yes: at strong inter-channel coupling, the current pulse associated with a single electron excitation is expected to split into two current pulses propagating at the slow and fast velocities and carrying a fractional charge²¹⁻²³. Recent time resolved measurements of electrical currents have confirmed this picture for two counter-propagating edge channels²⁴. On the other hand, the energy relaxation does not show such a splitting between charge and spin: the energy resolved excitation disappears into a wave of electron/hole excitations^{9,25}. As we shall see in this Let-

ter, the proper way to reconcile these two apparently discording points of view is to work within the Wigner function approach²⁶ thus gaining access to both the time course and energy content of single electron coherence.

To this end, we consider the relaxation of an arbitrary single electron excitation described by a many-body state $|\varphi_e, F\rangle = \int \varphi_e(x)\psi^\dagger(x)|F\rangle dx$ involving an arbitrary normalized purely electronic wave packet $\varphi_e(x)$ above the Fermi sea $|F\rangle$. The quantity of interest is the single electron coherence $\mathcal{G}_{\rho,x}^{(e)}(t, t') = \langle \psi^\dagger(x, t')\psi(x, t) \rangle_\rho$ at position x and in the time domain^{9,27}. In the present letter, the excitation is injected into an interaction region as depicted on Fig. 1. Our main result is the non-perturbative computation of the outgoing single electron coherence (x in the out region) in terms of the incoming wave packet $\varphi_e(x)$ and of the interactions. To visualize the result, the Wigner function defined as²⁶:

$$W_{\rho,x}^{(e)}(t, \omega) = \int v_F \mathcal{G}_{\rho,x}^{(e)}\left(t + \frac{\tau}{2}, t - \frac{\tau}{2}\right) e^{i\omega\tau} d\tau \quad (1)$$

provides a very convenient real-valued representation for the single electron coherence. It describes the nature of excitations (electron-like for $\omega > 0$ and hole-like for $\omega < 0$) as well as real time aspects: both the electron distribution function $f_e(\omega)$ and the average electrical current $\langle i(x, t) \rangle$ are marginal distributions of the Wigner function, respectively obtained by averaging over time or integrating over ω ²⁶. The Wigner function contains a Fermi sea contribution ensuring that $W^{(e)}(t, \omega) \rightarrow 1$ when $\omega \rightarrow -\infty$ and the excess Wigner function $\Delta W_{\rho,x}^{(e)}(t, \omega)$ defined by subtracting the Fermi distribution function at the chemical potential at position x thus represents the contribution of excitations.

Panel (a) of Fig. 2 presents the excess Wigner function of the Landau single electron excitation of duration $\tau_e = \gamma_e^{-1}$ injected at an energy $\hbar\omega_e$ above the Fermi level. Since $\omega_e/\gamma_e = 10$, it is well separated from the Fermi sea. The corresponding Lorentzian peak of the excess electron distribution function $\delta f_e(\omega)$ can be seen on panel (c) of Fig. 4 while the corresponding current pulse is shown on panel (a). By contrast, the excess Wigner function of a Levitov excitation depicted on Panel (a) of Fig. 3 is not well separated from the Fermi sea. Both of them are purely electronic: they vanish in the half plane $\omega < 0$ corresponding to hole excitations.

Let us now send such a coherent single electron excitation through an interaction region of finite length as shown on Fig. 1. Within this region, electrons experience screened Coulomb interactions with neighboring edge channels, other mesoscopic conductors and gates. In many experimentally relevant cases, such effective interactions can be described in terms of edge-magnetoplasmon scattering²⁸⁻³⁰ which are charge density waves along the edge channel. Assuming that all conductors involved are in the linear response regime when a single electron excitation passes through, this scattering is elastic. In this simple picture depicted on

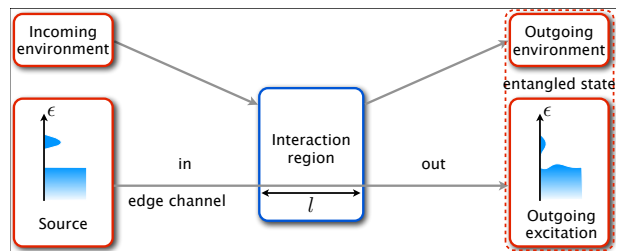


FIG. 1: A single electron excitation prepared in a coherent wave packet φ_e enters a finite length interaction region. The edge channel comes out entangled with the environmental degrees of freedom. In the case of two edge channels, the second channel plays the role of the environment.

Fig. 1, an incoming sinusoidal charge density wave at pulsation ω generates excitations at the same frequency in the environmental modes through the capacitive coupling between the edge channel and its electromagnetic environment. Under this hypothesis, the evolution of the many-body state $|\varphi_e, F\rangle$ can be completely described in terms of the edge magnetoplasmon transmission amplitude $t(\omega)$ ²⁵. This also suggests that interactions are most conveniently handled in the frequency domain.

Our key result is an analytical expression for the outgoing single electron coherence in the frequency domain $\tilde{\mathcal{G}}_{\text{out}}^{(e)}(\omega + \Omega/2, \omega - \Omega/2)$ where ω and Ω are respectively conjugated to $t - t'$ and $(t + t')/2$ in $\mathcal{G}_{\text{out}}^{(e)}(t, t')$. The outgoing coherence is obtained in terms of the excess coherence of the incoming wave packet

$$\tilde{\mathcal{G}}_{\text{out}}^{(e)}\left(\omega + \frac{\Omega}{2}, \omega - \frac{\Omega}{2}\right) = \int_{-\infty}^{+\infty} K(\omega, \omega'; \Omega) \tilde{\varphi}_e\left(\omega' + \frac{\Omega}{2}\right) \tilde{\varphi}_e^*\left(\omega' - \frac{\Omega}{2}\right) d\omega' \quad (2)$$

in which the propagator $K(\omega, \omega'; \Omega)$ encodes the effect of interactions on single electron excitations and $\tilde{\varphi}_e(\omega)$ denotes the Fourier transform of $\varphi_e(-v_F t)$. Contrary to the expressions obtained for energy resolved single electron excitations²⁵, Eq. (2) and the analytical expressions for $K(\omega, \omega'; \Omega)$ given in appendix B describe both the time and energy dependence of electronic relaxation. They provide the exact solution to the relaxation and decoherence problem for any incoming single electronic wave packet and for generic effective screened Coulomb interactions described within the framework of elastic edge magnetoplasmon scattering. In this Letter, we focus on the case of the $\nu = 2$ edge channel system with short range interactions, at strong coupling²⁰ and zero temperature (see appendix A).

Numerical evaluations of the outgoing Wigner function for an incoming Lorentzian wavepacket in the energy domain centered around $\hbar\omega_e$ and of width $\gamma_e = \tau_e^{-1}$ are depicted on Fig. 2 for various propagation distances or, equivalently, times of flight. These results shed light on the decoherence scenario of the Landau quasi-particle: it

clearly involves a time scale separation. In the limit of an energy resolved wave packet $\gamma_e \ll \omega_e$, the single electron coherence around ω_e relaxes close to the Fermi level after a propagation distance proportional to ω_e^{-1} . Then, after a propagation distance proportional to the wave packet duration $\gamma_e^{-1} \gg \omega_e^{-1}$, the single electron coherence splits into two parts progressing at the velocities of the two edge magnetoplasmon eigenmodes, thus giving birth to collective excitations close to the Fermi sea. The first phenomenon is indeed associated with energy relaxation probed by Le Sueur *et al*¹⁷ whereas the second one corresponds to the expected charged/neutral mode separation probed by Bocquillon *et al*¹⁹. This decoherence scenario should be compared to the one for the Leviton quasiparticle shown on Fig. 3: the Leviton splits into two half-Levitons which are Lorentzian current pulses carrying a charge $-e/2$. The only time scale appearing corresponds to the time needed to fractionalize a Leviton^{21–23}.

The difference between these two situations arises from the nature of the incoming many-body states: for the Leviton, it is a coherent state of the edge magnetoplasmon modes or, equivalently, a quasi-classical charge density wave²¹. Since the interaction region acts as a frequency dependent beam splitter for the edge magnetoplasmons, the Leviton many-body state does not entangle with environmental degrees of freedom. In other words, it is a pointer state³¹ which does not experience decoherence. The Wigner function changes shown on Fig. 3 come from electron/hole pair generation in this pure many-body state.

On the other hand, the many-body state corresponding to the Landau quasi-particle is a coherent superposition of such pointer states. It is thus subject to decoherence induced by entanglement with the second edge channel. Depending on the copropagation distance, the outgoing many-body state of the edge channel under consideration is a partly decohered mixture of coherent states, each of them corresponding to a localized electronic excitation dressed by a cloud of electron-hole pairs (see appendix B). This extrinsic decoherence manifests itself through the rapid decay of the Wigner function at the initial injection energy $\hbar\omega_e$.

Therefore, the rapid electronic relaxation shown on Fig. 2 should be viewed as the electronic analogue of the decay of interference fringes expected for the Wigner function of the superposition of two coherent states of an electromagnetic mode recently observed in cavity QED experiments³². Here, it arises from the decoherence of a mesoscopic superposition of quasi-classical charge density waves. This process takes place over a shorter time than the evolution of each of these quasi-classical states which corresponds to the spin-charge separation of the current pulses. Once this decoherence process has taken place, the outgoing many-body state is an incoherent mixture of fractionalized localized electronic excitations. We confirm this scenario by computing both the current pulse and the electron distribution function corresponding to each of the Wigner functions of Fig. 2: the decay of the

quasi-particle peak takes place at short times (Fig. 4c). During this time the current pulses are almost unseparated (Fig. 4a) and no hole excitations are created, thus confirming that it is a purely extrinsic decoherence effect. As the separation of the two half-charge current pulses becomes more visible (Fig. 4b), hole excitations are created (Fig. 4d).

For typical duration of the wave packet generated by single electron sources⁸ $\tau_e \simeq 60$ ps and typical velocity of the slow mode¹⁹ $v_s \simeq 4.6 \times 10^4$ m s⁻¹, energy relaxation takes place over a propagation distance smaller than $v_s \tau_e \simeq 2.8$ μ m. Therefore, without any decoherence/relaxation preserving design^{15,33}, the single electron coherence measured after a few μ m propagation along a second edge channel corresponds to collective excitations close to the Fermi sea such as the one depicted on panel (f) of Fig. 2. This decay of single electron coherence is responsible for the reduction of contrast in MZI interferometry experiments^{20,34}. Moreover, as pointed out by Wahl *et al*³⁵, interactions also lead to a reduction of the Pauli dip in HOM experiments, as recently observed⁸.

Since the experimental signal in an Hong-Ou-Mandel interferometer is directly related to the overlap of the two incoming excess Wigner functions²⁶, HOM experiments can efficiently probe the outgoing single electron coherence with sub-nanosecond time resolution. First of all, the side peak structures in the HOM signal predicted by Wahl *et al*³⁵ reflect the splitting of the outgoing collective excitation Wigner function with increasing propagation distance as can be seen on panels (d) to (f) of Fig. 2. But more generally, using for example very narrow Lorentzian pulses⁴² and a d.c. bias, an HOM-like experiment would probe the precise time and frequency dependence of the outgoing Wigner function. Anti-Levitons (Lorentzian pulses carrying charge $+e$) could be used to probe both the time and frequency dependence of the outgoing Wigner function for $\omega < 0$ and the corresponding HOM signal may exhibit contributions from the electron/hole coherences generated by interactions³⁶. Finally, the edge magnetoplasmon decoherence manifests itself through a striking phenomenon: once it has taken over, because all contributions arising from the initial coherence $\varphi_e(t_+) \varphi_e^*(t_-)$ at different times $t_+ \neq t_-$ are suppressed, the outgoing single electron coherence only depends on $|\varphi_e(t)|^2$. Consequently, it only depends on the shape of the incoming current pulse and not on its injection energy. This striking feature can be easily tested in an HOM experiment: the HOM curve should not change when modifying the injection energy of the electron while keeping the duration of the wave packet constant as long as it is injected well above the Fermi level. The precise shape of this curve does however depend on the form of effective interactions¹⁹. This dependence as well as the effect of non-zero temperature will be explored in a subsequent publication.

To conclude, we have computed the Wigner function of a coherent single electron excitation after propagating across an interaction region of the $\nu = 2$ edge channel

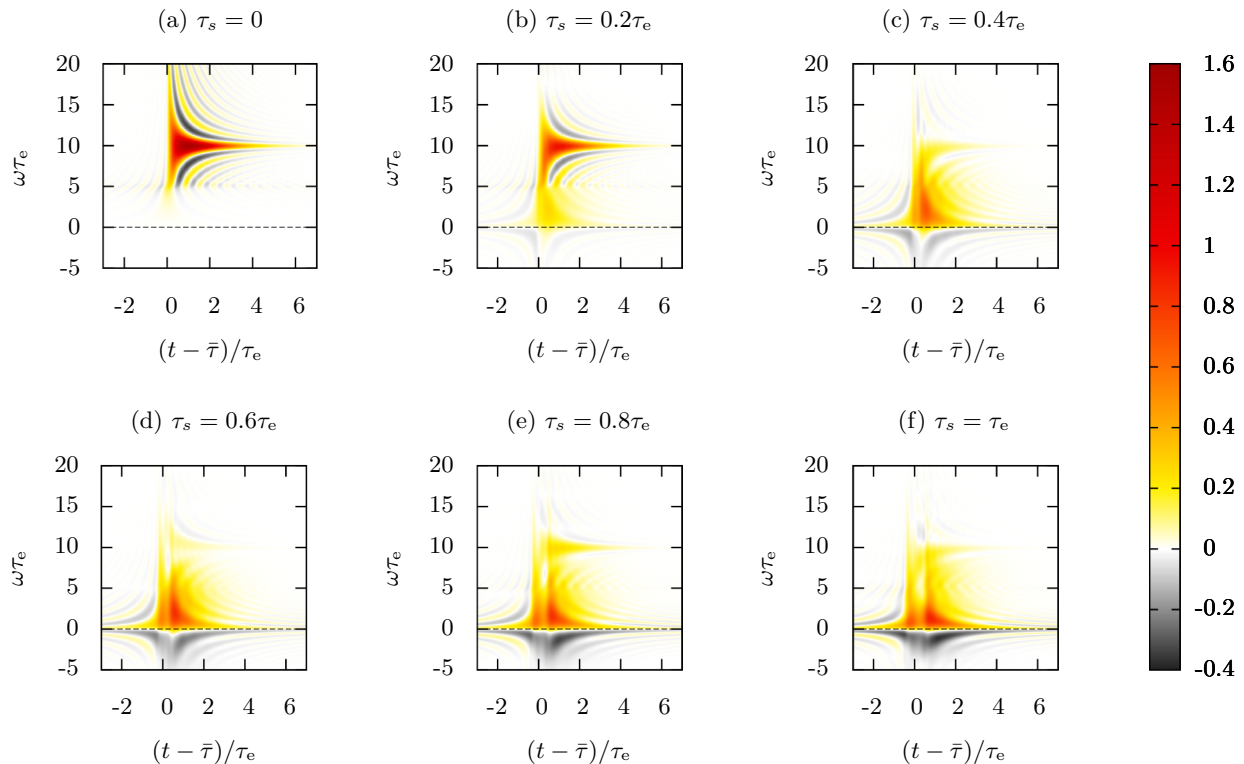


FIG. 2: (Color online) Excess Wigner function $\Delta W_{\text{out}}^{(e)}(t, \omega)$ at various propagation times for a Lorentzian wave packet in energy (Landau excitation) of lifetime $\tau_e = \gamma_e^{-1}$ emitted at energy $\hbar\omega_e = 10\hbar\tau_e^{-1}$. The Fermi level is indicated as an horizontal dashed line at $\omega = 0$. The various plots correspond to increasing propagating lengths expressed in terms of times of flight: τ_s for the slow mode and $\tau_c = \tau_s/20$ corresponds to the fast mode. The time shift $\bar{\tau} = (\tau_c + \tau_s)/2$ compensates for the global drift of the excitations. The initial excess Wigner function is depicted on panel (a). Most of the electronic relaxation takes place at short times of flight (panels (a) to (c)) whereas the spin-charge separation appears over longer times of flight (panels (d) to (f)).

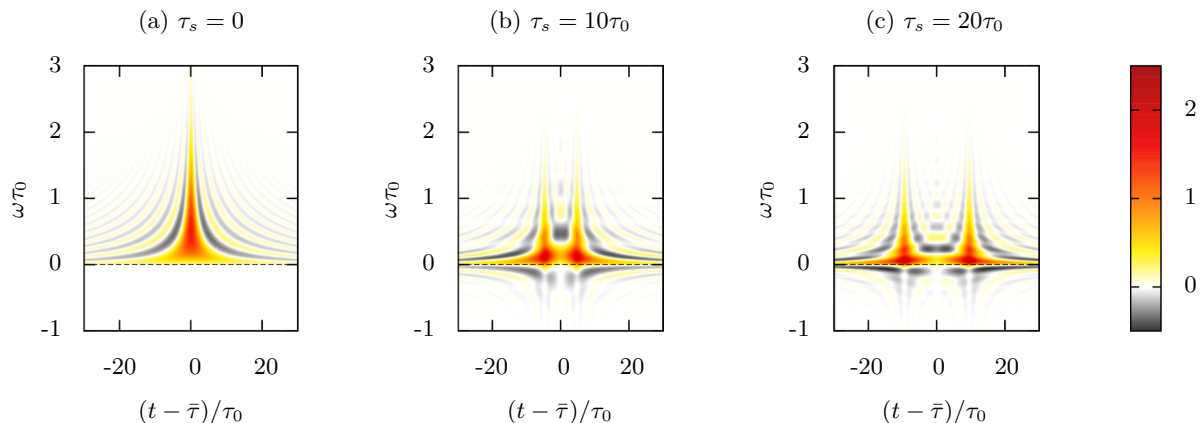


FIG. 3: (Color online) Excess Wigner function $\Delta W_{\text{out}}^{(e)}(t, \omega)$ of a single electronic Leviton of width τ_0 for various propagation times: τ_s (resp. τ_c) denotes the time of flight of the spin (resp. charged) mode within the interaction region and $\tau_c = \tau_s/20$ and $\bar{\tau} = (\tau_s + \tau_c)/2$. The incoming Leviton splits into two half-Levitons which are collective excitations.

system. We have unraveled fundamental difference between the decoherence scenario of the Landau and Leviton quasi-particles that reflects the decoherence of the corresponding final many-body states. We suggest that HOM type experiments could probe the incoherent mixture of fractionalized localized electronic excitations resulting from the effect of Coulomb interactions on the

Landau quasi-particle. In particular, we propose a simple test of this decoherence based on the HOM experiment. These experimental tests would provide useful information on the decoherence mechanisms and effective interactions at a much lower experimental cost than the generic tomography protocols based on HBT³⁸ or MZI³⁹ interferometry.

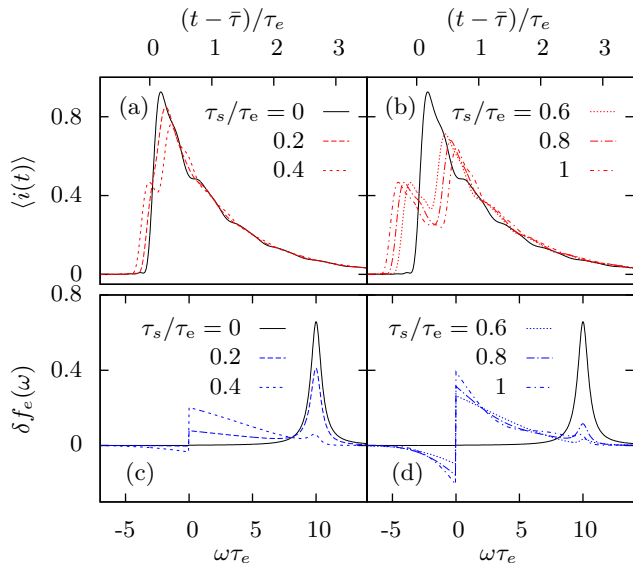


FIG. 4: (Color online) We present the average current $\langle i(t) \rangle$ in units of $-e/\tau_e$ (top row) and the excess electron distribution function $\delta f_e(\omega)$ (bottom row) at the same propagation distances as on Fig. 2 for an initial Lorentzian wave packet in energy (Landau excitation) of lifetime $\tau_e = \gamma_e^{-1}$ and energy $\hbar\omega_e = 10\hbar\tau_e^{-1}$. The initial $\langle i(t) \rangle$ and $\delta f_e(\omega)$ appear as filled black curves on all panels. For short propagation times (panels (a) and (c)), the current peaks are not very well separated and no hole excitations are created but the quasi-particle peak in the electron distribution function strongly decays. For longer propagation times (panels (b) and (d)), hole excitations appear as the current pulse fractionalizes in two well separated peaks whereas the quasi-particle peak remains small.

Acknowledgments

We thank J.M. Berroir, E. Bocquillon, V. Freulon and B. Plaçais from LPA for useful discussions as well as C. Bauerle from Institut Neel. We also thank T. Jonckheere, T. Martin, J. Rech and C. Wahl from CPT Marseille for discussions about their work and for very useful remarks on our manuscript. This work is supported by the ANR grant "1shot" (ANR-2010-BLANC-0412).

Appendix A: Interactions and edge-magnetoplasmon scattering

In this paper, we consider the $\nu = 2$ edge channel system and review the description of screened Coulomb interactions in terms of edge magnetoplasmon scattering. To begin with, let us, in full generality, consider a quantum Hall edge channel capacitively coupled to a linear environment such as, for example, an external gate of size l connected to an impedance representing a dissipative circuit²⁵ or a second edge channel^{20,30}. The interaction region is assumed to be of finite length. Solving the equations of motion for the bosonic degree of freedom describing the edge channel (edge magnetoplasmon

modes) and the environmental bosonic modes then leads to an elastic scattering matrix that describes the effect of the interaction region on both the edge-magnetoplasmon and the environmental modes. The precise form and frequency dependence of this matrix depends on the precise form of effective Coulomb interactions used in the model. The edge magnetoplasmon scattering matrix is indeed related to the finite frequency admittances of the conductors^{25,28,29}, thus enabling an experimental determination of such plasmon scattering amplitudes¹⁹.

We now focus on two copropagating edge channels coupled over a distance l by short range effective screened Coulomb interactions. Over a copropagation distance l , such short range interactions lead to the dispersionless propagation of the two edge magnetoplasmon modes which are called the slow and the fast modes with respective velocities v_s and v_c ($v_c > v_s$). The interaction strength is characterized by a single angular parameter θ which determines how these eigenmodes are expressed as linear combinations of the edge magnetoplasmon modes of the two edge channels. Importantly, the strong coupling regime corresponds to $\theta = \pi/2$ ²⁰. In this regime, the fast mode is symmetric and therefore carries the total charge: this is why we denote it by the subscript c . The slow mode is then neutral and corresponds to opposite charges on both edges. For this reason, the neutral mode is often called dipolar or, assuming that both edge channels carry opposite spins in the quantization direction given by the magnetic field, the spin mode. This leads to the following edge-magnetoplasmon scattering³⁰:

$$S(\omega) = \begin{pmatrix} p_s e^{i\omega\tau_s} + p_c e^{i\omega\tau_c} & q (e^{i\omega\tau_c} - e^{i\omega\tau_s}) \\ q (e^{i\omega\tau_c} - e^{i\omega\tau_s}) & p_c e^{i\omega\tau_s} + p_s e^{i\omega\tau_c} \end{pmatrix}, \quad (\text{A1})$$

where $\tau_s = l/v_s$ and $\tau_c = l/v_c$ respectively denotes the time of flight of the slow and fast modes and

$$p_{s/c} = \frac{1 \pm \cos(\theta)}{2}, \quad q = \frac{\sin(\theta)}{2}. \quad (\text{A2})$$

Because the edge magnetoplasmon modes are dispersionless, the charge density wave generated by applying a time dependent voltage drive to one of the two edge channels propagates in a very simple way: a classical drive generates an edge magnetoplasmon coherent state which thus propagates just as a classical electromagnetic wave through a frequency dependent beam splitter. As a consequence, the outgoing quantum state is just a tensor product of two edge magnetoplasmon states that correspond to the outgoing transmitted and reflected waves²¹. Fig. 5 depicts the result of this process for an incoming Lorentzian pulse in the time or space domain such as, for example, the recently generated Leviton quasi-particle or Leviton⁴: due to the absence of dispersion for the fast and slow eigenmodes²¹, this excitation splits into two Lorentzian pulses with half amplitude.

Recently, finite frequency admittance measurements by Bocquillon *et al*¹⁹ have shown that this picture is valid

at low energies and that the eigenmodes correspond to the strong coupling case $\theta = \pi/2$. Fractionalization has also been recently confirmed by Heiblum *et al* through noise measurements but with a different mixing angle ($\theta \simeq \pi/3$)⁴⁰. Nevertheless, we shall focus on the strong coupling case in this paper.

Appendix B: Computing single electron coherence

We shall now present the method used to compute the single electron excess coherence coming out of the interaction region. The analytical expressions used for numerical evaluations are valid at zero temperature, for arbitrary incoming single electron wave packet and for arbitrary effective interactions described by edge magnetoplasmon scattering. We proceed by deriving numerical expressions for the excess single electron coherence

$$\mathcal{G}_{\text{out}}^{(e)}\left(t + \frac{\tau}{2}, t - \frac{\tau}{2}\right) = v_F^2 \int \varphi_e(t_+) \varphi_e(t_-)^* \left\langle \psi(t_-) \psi^\dagger\left(t - \frac{\tau}{2}\right) \psi\left(t + \frac{\tau}{2}\right) \psi^\dagger(t_+) \right\rangle_F dt_+ dt_- \quad (\text{B2})$$

where $\langle A \rangle_F$ denotes the quantum average of A in the Fermi sea $|F\rangle$. Using Wick's theorem, the incoming single electron contribution is obtained as the sum of two

$$\mathcal{G}_{\text{in}}^{(e)}\left(t + \frac{\tau}{2}, t - \frac{\tau}{2}\right) = \mathcal{G}_F^{(e)}(\tau) + \mathcal{G}_{\text{in,wp}}^{(e)}\left(t + \frac{\tau}{2}, t - \frac{\tau}{2}\right) \quad (\text{B3a})$$

$$\mathcal{G}_{\text{in,wp}}^{(e)}\left(t + \frac{\tau}{2}, t - \frac{\tau}{2}\right) = v_F^2 \int \varphi_e(t_+) \varphi_e(t_-)^* \left\langle \psi\left(t + \frac{\tau}{2}\right) \psi^\dagger(t_+) \right\rangle_F \left\langle \psi\left(t - \frac{\tau}{2}\right) \psi^\dagger(t_-) \right\rangle_F^* dt_+ dt_- \quad (\text{B3b})$$

where $\mathcal{G}_F^{(e)}(\tau) = \langle \psi^\dagger(0) \psi(\tau) \rangle_F$ denotes the single electron coherence of the Fermi sea. Since we consider a purely electronic wave packet φ_e the two point fermionic correlators can safely be replaced by δ functions, thus leading to the familiar expression for the excess single electron coherence $\Delta\mathcal{G}^{(e)} = \mathcal{G}^{(e)} - \mathcal{G}_F^{(e)}$:

$$\Delta\mathcal{G}_{\text{in}}^{(e)}\left(t + \frac{\tau}{2}, t - \frac{\tau}{2}\right) = \varphi_e\left(t + \frac{\tau}{2}\right) \varphi_e\left(t - \frac{\tau}{2}\right)^* . \quad (\text{B4})$$

$$\mathcal{G}_{\text{out}}^{(e)}\left(t + \frac{\tau}{2}, t - \frac{\tau}{2}\right) = v_F^2 \int \varphi_e(t_+) \varphi_e(t_-)^* \mathcal{D}_{\text{ext}}(t_+ - t_-) \left\langle g(t_-) \left| \psi(t_-) \psi^\dagger\left(t - \frac{\tau}{2}\right) \psi\left(t + \frac{\tau}{2}\right) \psi^\dagger(t_+) \right| g(t_+) \right\rangle dt_+ dt_- . \quad (\text{B5})$$

where $\mathcal{D}_{\text{ext}}(t_+ - t_-)$ is the extrinsic decoherence coefficient that arises from the imprints left in the external en-

vironment by localized fermionic excitations located at t_+

in the frequency domain. The excess Wigner function²⁶ is then evaluated by performing a discrete Fourier transform (DFT).

1. Computing the outgoing single electron coherence

Let us consider an incoming many-body state of the form

$$|\varphi_e, F\rangle = v_F \int \varphi_e(t) \psi^\dagger(t) |F\rangle dt \quad (\text{B1})$$

where $\varphi_e(t)$ denotes the electronic wave packet evaluated at $x = -v_F t$. The resulting incoming single electron coherence is then obtained as a double integral involving a four point fermionic correlator:

contributions, one corresponding to the Fermi sea and one corresponding to the electronic wave packet:

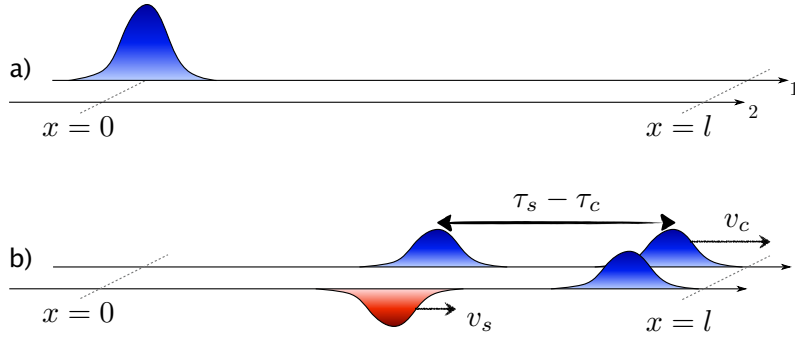


FIG. 5: Propagation of a Lorentzian pulse in the $\nu = 2$ edge channel system in the presence of short range interactions at strong coupling: (a) a Lorentzian pulse is injected on one of the two edge channels before the interaction region; (b) this excitation has been fractionalized leading to a fast moving charge excitation c and a slow moving neutral excitation s .

and t_- . It is given in terms of the scattering probability $R(\omega)$ of an edge magnetoplasmon into the environmental modes at the same frequency²⁵:

$$\mathcal{D}_{\text{ext}}(\tau) = \exp\left(\int_0^{+\infty} R(\omega) (e^{i\omega\tau} - 1) \frac{d\omega}{\omega}\right) \quad (\text{B6})$$

in which $R(\omega) = |S_{12}(\omega)|^2$. The states $|g(t_{\pm})\rangle$ in Eq. (B5) are the edge magnetoplasmon coherent states describing the corresponding electron/hole pair clouds generated

into the edge channels by screened Coulomb interactions:

$$|g(t_{\pm})\rangle = \bigotimes_{\omega>0} \left| \frac{e^{i\omega t_{\pm}}}{\sqrt{\omega}} (1 - t(\omega)) \right\rangle. \quad (\text{B7})$$

where $t(\omega) = S_{11}(\omega)$ denotes the edge magnetoplasmon transmission amplitude. This finally leads to an expression for the outcoming single electron coherence that generalizes Eq. (B2) as:

$$\mathcal{G}_{\text{out}}^{(e)}\left(t + \frac{\tau}{2}, t - \frac{\tau}{2}\right) = v_F^2 \int \varphi_e(t_+) \varphi_e(t_-)^* \left\langle \psi(t_-) \psi^\dagger\left(t - \frac{\tau}{2}\right) \psi\left(t + \frac{\tau}{2}\right) \psi^\dagger(t_+) \right\rangle_F \mathcal{D}_{t_+, t_-}(t, \tau) dt_+ dt_- \quad (\text{B8})$$

where the full decoherence coefficient $\mathcal{D}_{t_+, t_-}(t, \tau)$ takes into account both the effect of extrinsic decoherence and of the overlap of the accompanying clouds of electron hole pairs. It also takes into account the effect of the time dependent electrical potential generated by these coherent electron/hole pairs: this potential acts as a quan-

tum phase on the electrons. Due to time translation invariance of the dynamics, it is relevant to decompose $t_{\pm} = \bar{t} \pm \bar{\tau}/2$ since in this case $\mathcal{D}_{\bar{t} + \bar{\tau}/2, \bar{t} - \bar{\tau}/2}(t, \tau)$ only depends on τ , $\bar{\tau}$ and $t - \bar{t}$. The full decoherence coefficient is finally equal to:

$$\begin{aligned} \mathcal{D}_{\bar{t} + \bar{\tau}/2, \bar{t} - \bar{\tau}/2}(t, \tau) &= \exp\left(\int_0^{+\infty} (1 - t^*(\omega)) e^{i\omega(t - \bar{t})} \left[e^{i\omega\tau/2} - e^{-i\omega\tau/2} \right] e^{i\omega\bar{\tau}/2} \frac{d\omega}{\omega}\right) \\ &\times \exp\left(\int_0^{+\infty} (1 - t(\omega)) e^{-i\omega(t - \bar{t})} \left[e^{-i\omega\tau/2} - e^{i\omega\tau/2} \right] e^{i\omega\bar{\tau}/2} \frac{d\omega}{\omega}\right). \end{aligned} \quad (\text{B9})$$

In the case of short range interactions, Eqs. (B8) and (B9) lead to an expression for the outcoming single electron coherence involving algebraic functions whose infrared divergences are not easy to control³⁵. In order

to evaluate the outcoming single electron coherence, it is then more convenient to go to the frequency domain and to use Wick's theorem to decompose the four point correlator in Eq. (B8) as a sum of products of two point

correlators. Moreover, this method enables treating various effective interactions. It opens the way to the comparison of their effect on electronic decoherence as will be discussed in a forthcoming publication.

The outgoing single electron coherence is thus obtained as a sum of two contributions which generalize the decomposition given by Eqs. (B3a) and (B3b) in the case where interactions are present:

$$\mathcal{G}_{\text{out}}^{(e)}\left(t + \frac{\tau}{2}, t - \frac{\tau}{2}\right) = \mathcal{G}_{\text{out,mv}}^{(e)}\left(t + \frac{\tau}{2}, t - \frac{\tau}{2}\right) + \mathcal{G}_{\text{out,wp}}^{(e)}\left(t + \frac{\tau}{2}, t - \frac{\tau}{2}\right) \quad (\text{B10a})$$

$$\mathcal{G}_{\text{out,mv}}^{(e)}\left(t + \frac{\tau}{2}, t - \frac{\tau}{2}\right) = \int \varphi_e(t_+) \varphi_e(t_-)^* K_{\text{mv}}(t, \tau | t_+, t_-) dt_+ dt_- \quad (\text{B10b})$$

$$\mathcal{G}_{\text{out,wp}}^{(e)}\left(t + \frac{\tau}{2}, t - \frac{\tau}{2}\right) = \int \varphi_e(t_+) \varphi_e(t_-)^* K_{\text{wp}}(t, \tau | t_+, t_-) dt_+ dt_- . \quad (\text{B10c})$$

The two propagators K_{mv} and K_{wp} are given in the time domain by:

$$K_{\text{mv}}(t, \tau | t_+, t_-) = v_F^2 \left\langle \psi^\dagger\left(t - \frac{\tau}{2}\right) \psi\left(t + \frac{\tau}{2}\right) \right\rangle_F \langle \psi(t_-) \psi^\dagger(t_+) \rangle_F \mathcal{D}_{t_+, t_-}(t, \tau) \quad (\text{B11a})$$

$$K_{\text{wp}}(t, \tau | t_+, t_-) = v_F^2 \left\langle \psi\left(t + \frac{\tau}{2}\right) \psi^\dagger(t_+) \right\rangle_F \left\langle \psi^\dagger\left(t - \frac{\tau}{2}\right) \psi(t_-) \right\rangle_F^* \mathcal{D}_{t_+, t_-}(t, \tau) \quad (\text{B11b})$$

In the case of weak interactions with limited bandwidth, the two contributions to single electron coherence are well separated²⁵: Eq. (B11a) contains the Fermi sea agitated by the electron/hole pairs generated by the incoming electronic excitation through effective Coulomb interactions whereas Eq. (B11b) encodes the contribution of the incoming single electron excitation experiencing

relaxation.

Due to time translation invariance, the propagator expressed in the time domain only depends on τ , $\bar{\tau}$ and the time difference $t - \bar{t}$. Consequently, in the frequency domain, we have:

$$\mathcal{G}_{\text{mv}}^{(e)}\left(\omega + \frac{\Omega}{2}, \omega - \frac{\Omega}{2}\right) = \int_{-\infty}^{+\infty} \tilde{\varphi}_e\left(\omega' + \frac{\Omega}{2}\right) \tilde{\varphi}_e^*\left(\omega' - \frac{\Omega}{2}\right) K_{\text{mv}}(\omega, \omega'; \Omega) d\omega' \quad (\text{B12a})$$

$$\mathcal{G}_{\text{wp}}^{(e)}\left(\omega + \frac{\Omega}{2}, \omega - \frac{\Omega}{2}\right) = \int_{-\infty}^{+\infty} \tilde{\varphi}_e\left(\omega' + \frac{\Omega}{2}\right) \tilde{\varphi}_e^*\left(\omega' - \frac{\Omega}{2}\right) K_{\text{wp}}(\omega, \omega'; \Omega) d\omega' \quad (\text{B12b})$$

where $K_{\text{mv}}(\omega, \omega'; \Omega)$ and $K_{\text{wp}}(\omega, \omega'; \Omega)$ are the Fourier transforms of the two propagators defined by Eqs. (B11a) and (B11b) with respect to τ , $\bar{\tau}$ and $t - \bar{t}$. The complete propagator that appears in Eq. (2) of the paper is then $K(\omega, \omega'; \Omega) = K_{\text{mv}}(\omega, \omega'; \Omega) + K_{\text{wp}}(\omega, \omega'; \Omega)$. We shall now derive their explicit expressions which have been used to obtain the numerical results presented in the paper.

2. Explicit expressions

a. The free propagators

To begin with, for vanishing interactions, $\mathcal{D}_{t_+, t_-}(t, \tau) = 1$. In this case, the coherence prop-

agators can easily be evaluated:

$$K_{\text{mv}}^{(0)}(\omega, \omega'; \Omega) = 2\pi\delta(\Omega) f_F(\omega) (1 - f_F(\omega')) \quad (\text{B13a})$$

$$K_{\text{wp}}^{(0)}(\omega, \omega'; \Omega) = 2\pi\delta(\omega - \omega') \left(1 - f_F\left(\omega + \frac{\Omega}{2}\right) \right) \times \left(1 - f_F\left(\omega - \frac{\Omega}{2}\right) \right) \quad (\text{B13b})$$

in which $f_F(\omega) = \Theta(-\omega)$ denotes the zero temperature Fermi function. The $\delta(\Omega)$ in Eq. (B13a) reflects the stationarity of $K_{\text{mv}}^{(0)}$ which at zero temperature, restores the Fermi sea contribution to single electron coherence. The $\delta(\omega - \omega')$ in Eq. (B13b) reflects the fact that, for vanishing interactions, no dissipative processes are present. Note that at zero temperature, $K_{\text{wp}}^{(0)}$ is non vanishing only when both $\omega_+ = \omega + \Omega/2$ and $\omega_- = \omega - \Omega/2$ are positive. In this case, $(\omega + \Omega/2, \omega - \Omega/2)$ is said to belong to the (e) quadrant²⁶. This contribution gives the excess single electron coherence associated with the incoming wave packet. Of course, we are interested in the excess single electron coherence and therefore, we shall always subtract the contribution $K_{\text{mv}}^{(0)}$ that leads to the Fermi sea from the propagator.

b. The interacting case: general properties of the propagators

In the interacting case, the decoherence coefficient $\mathcal{D}_{t_+, t_-}(t, \tau)$ is no longer equal to unity and should therefore be taken into account. Fig. 6 depicts how the coherence of the incoming wave packet contributes to the outgoing excess coherence after the interaction region.

The initial coherence only contributes to the outgoing coherence at lower energies because we work at zero temperature and therefore there are no heating effects. Moreover, the incoming excess coherence at $(\omega' + \Omega/2, \omega' - \Omega/2)$ cannot contribute to the outgoing coherence at $(\omega + \Omega/2, \omega - \Omega/2)$ for $\omega < -\omega'$ since the incoming electron at energy $\hbar\omega' > 0$ cannot generate an electron/hole pair excitation of energy higher than $\hbar\omega'$. The Pauli exclusion principle then leads to the selection rule $K(\omega, \omega'; \Omega) = 0$ for $\omega < -\omega'$.

c. Basic blocks

Apart from the case of free propagation, it is impossible to find closed compact expressions for these propagators. Consequently, a numerical evaluation has to be performed which, as we shall see now, can be quite challenging and requires a careful methodology to be both effective and accurate.

As explained before, the best strategy is to evaluate the propagators in the frequency domain. In the interacting case, the novelty comes from the decoherence coefficient

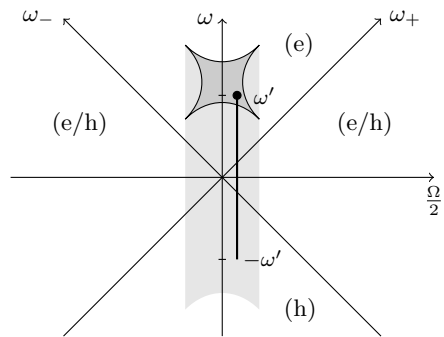


FIG. 6: Propagation of single electron coherence in the frequency domain: the coherence of the incoming electronic wavepacket at $(\omega' + \Omega/2, \omega' - \Omega/2)$ ($\omega' > 0$) contributes to the excess outgoing coherence at $(\omega + \Omega/2, \omega - \Omega/2)$ for $-\omega' \leq \omega \leq \omega'$ (points belonging to the vertical black line). Grey zone: localization of the incoming single electron coherence in the frequency domain for a Landau quasi-particle. Light grey zone: localization of the excess outgoing single electron coherence. The frequency domain is divided in four quadrants²⁶: two of them corresponding respectively to electron (e) and hole (h) excitations and two off-diagonal quadrants associated with electron/hole (e/h) coherences. Interactions are expected to generate both of them from an incoming excitation located within the (e) quadrant.

$\mathcal{D}_{\bar{\tau}/2, -\bar{\tau}/2}(t + \tau/2, t - \tau/2)$. Its Fourier transform with respect to τ , $\bar{\tau}$ and t can be obtained as a convolution involving the Fourier transforms:

$$\Gamma_{\pm}(\omega) = \int_{-\infty}^{+\infty} e^{i\omega t} \exp\left(\pm \int_0^{+\infty} (1 - t(\omega'))(e^{i\omega' t} - 1) \frac{d\omega'}{\omega'}\right) dt. \quad (\text{B14})$$

Assuming that

$$\Lambda_{\pm} = \exp\left(\mp \int_0^{+\infty} (1 - t(\omega)) \frac{d\omega}{\omega}\right)$$

is finite and non zero, which can always be ensured by a suitable UV regularization since it is known that $t(\omega) - 1 \simeq O(\omega)$ at $\omega \rightarrow 0^+$, these Fourier transforms have a δ singularity at $\omega = 0$ and a regular part for $\omega < 0$:

$$\Gamma_{\pm}(\omega) = 2\pi\Lambda_{\pm} (\delta(\omega) + B_{\pm}(-\omega)) \quad (\text{B15})$$

where $B_{\pm}(\omega)$ are regular functions vanishing for $\omega < 0$. As we shall see, once the functions B_{\pm} are known, the Fourier transform of the decoherence coefficient is known.

More precisely, using the decomposition given by Eq. (B15), the Fourier transform of the decoherence coefficient $\mathcal{D}_{\bar{\tau}/2, -\bar{\tau}/2}(t, \tau)$ with respect to τ , $\bar{\tau}$ and t can be decomposed as a sum of $2^4 = 16$ terms. Therefore, each of the propagators is also a sum of 16 terms. One among the 16 terms of the modified vacuum propagator contains the Fermi sea contribution. Therefore, the analytic expressions for the full propagator giving the excess outgoing single electron coherence involve 31 terms which will be detailed in the present section. Although quite

tedious, these expressions provide a perfect control of all the infrared singularities arising in a direct time domain computation at vanishing temperature³⁵. A generalization of these expressions at non-zero temperatures can be obtained but this would go beyond the scope of the present paper.

Before detailing these 31 terms, let us mention that both auxiliary functions $B_{\pm}(\omega)$ are evaluated for positive frequencies by solving numerically the following integral equations:

$$\omega B_{\pm}(\omega) = \pm \left[1 - t(\omega) + \int_0^{\omega} d\omega' B_{\pm}(\omega') (1 - t(\omega - \omega')) \right] \quad (\text{B16})$$

where the initial value $B_{\pm}(0^+)$ is defined using the deriva-

tives of $t(\omega)$:

$$B_{\pm}(0^+) = \pm \lim_{\omega \rightarrow 0^+} \frac{1 - t(\omega)}{\omega} = \mp t'(\omega = 0^+) \quad (\text{B17})$$

Expressions in the case of effective short range interactions in the $\nu = 2$ edge channel system are given in appendix C. They have been used to check the validity of the numerical solutions for B_{\pm} in this case.

d. The wave packet contribution

The wave packet contribution is a sum of two contributions of the following form:

$$\Delta \mathcal{G}_{\text{wp}}^{(e)} \left(\omega + \frac{\Omega}{2}, \omega - \frac{\Omega}{2} \right) = \tilde{\varphi}_e \left(\omega + \frac{\Omega}{2} \right) \tilde{\varphi}_e^* \left(\omega - \frac{\Omega}{2} \right) \mathcal{Z} \left(\omega + \frac{\Omega}{2} \right) \mathcal{Z}^* \left(\omega - \frac{\Omega}{2} \right) \quad (\text{B18a})$$

$$+ \int_{-\infty}^{+\infty} \tilde{\varphi}_e \left(\omega' + \frac{\Omega}{2} \right) \tilde{\varphi}_e^* \left(\omega' - \frac{\Omega}{2} \right) K_{\text{wp}}^{(\text{ne})}(\omega, \omega'; \Omega) d\omega' \quad (\text{B18b})$$

The first contribution Eq. (B18a) contains the purely elastic contribution corresponding to the electronic excitation going through the interaction region without experiencing any inelastic process. The elastic scattering amplitude $\mathcal{Z}(\omega_e)$ for an electron at incoming energy $\hbar\omega_e > 0$ is given by²⁵:

$$\mathcal{Z}(\omega_e) = 1 + \int_0^{\omega_e} B_{-}(\omega') d\omega'. \quad (\text{B19})$$

Let us recall that the inelastic scattering probability for the electron at initial energy $\hbar\omega_e$ is then given by

$$\sigma_{\text{in}}(\omega_e) = 1 - |\mathcal{Z}(\omega_e)|^2. \quad (\text{B20})$$

The second contribution, which contains the inelastic wave packet part $K_{\text{wp}}^{(\text{ne})}$ of the propagator, is given by:

$$K_{\text{wp}}^{(\text{ne})}(\omega, \omega'; \Omega) = B_{+}(\omega' - \omega) \mathcal{Z} \left(\omega + \frac{\Omega}{2} \right) \mathcal{Z}^* \left(\omega' - \frac{\Omega}{2} \right) + \text{conj.} \quad (\text{B21a})$$

$$+ \int_{-\infty}^{+\infty} B_{+}(k) B_{+}^*(\omega' - \omega - k) \mathcal{Z} \left(\omega' + \frac{\Omega}{2} - k \right) \mathcal{Z}^* \left(\omega - \frac{\Omega}{2} + k \right) dk \quad (\text{B21b})$$

where the notation $f(\Omega) + \text{conj.}$ should be understood as $f(\Omega) + f^*(-\Omega)$.

e. The modified vacuum contribution

The vacuum contribution to the excess single electron coherence K_{mv} is given by:

$$\Delta \mathcal{G}_{\text{mv}}^{(e)} \left(\omega + \frac{\Omega}{2}, \omega - \frac{\Omega}{2} \right) = \int_{-\infty}^{+\infty} K_{\text{mv}}(\omega, \omega'; \Omega) \times \tilde{\varphi}_e \left(\omega' + \frac{\Omega}{2} \right) \tilde{\varphi}_e^* \left(\omega' - \frac{\Omega}{2} \right) d\omega'. \quad (\text{B22})$$

The modified vacuum propagator $K_{\text{mv}}(\omega, \omega', \Omega)$ can be expressed as a sum of a part arising from singularities

and a part which involves no δ which is called the regular part:

$$K_{\text{mv}}(\omega, \omega'; \Omega) = K_{\text{mv}}^{(\text{sing})}(\omega, \omega'; \Omega) + \int_{\omega}^{+\infty} \mathcal{F}_{\text{mv}}^{(\text{reg})}(k, \omega'; \Omega) dk \quad (\text{B23})$$

The singular part is given by

$$K_{\text{mv}}^{(\text{sing})}(\omega, \omega'; \Omega) = B_-(\Omega) \Theta\left(-\omega + \frac{\Omega}{2}\right) + \text{conj.} \quad (\text{B24a})$$

$$+ B_+(\Omega) \Theta\left(-\omega - \frac{\Omega}{2}\right) + \text{conj.} \quad (\text{B24b})$$

$$+ \Theta\left(-\omega + \frac{\Omega}{2}\right) \int_0^{\infty} B_-\left(\omega' - k + \frac{\Omega}{2}\right) B_+^*\left(\omega' - k - \frac{\Omega}{2}\right) dk + \text{conj.} \quad (\text{B24c})$$

The various Heaviside functions Θ shows that $K_{\text{mv}}^{(\text{sing})}(\omega, \omega'; \Omega)$ corresponds to discontinuities at the boundaries between the (e) and (h) quadrants as

well as at the boundaries between the (e/h) and (h) quadrants²⁶. Finally, the regular part is the integral over k from ω to infinity of:

$$\mathcal{F}_{\text{mv}}^{(\text{reg})}(k, \omega'; \Omega) = B_+\left(-k + \frac{\Omega}{2}\right) B_-\left(k + \frac{\Omega}{2}\right) + \text{conj.} \quad (\text{B25a})$$

$$+ B_-\left(k + \frac{\Omega}{2}\right) B_-^*\left(k - \frac{\Omega}{2}\right) \Theta(\omega' - k) \quad (\text{B25b})$$

$$+ B_+\left(-k + \frac{\Omega}{2}\right) B_+^*\left(-k - \frac{\Omega}{2}\right) \Theta(\omega' + k) \quad (\text{B25c})$$

$$+ \int_0^{\infty} B_+^*\left(\omega' - q - \frac{\Omega}{2}\right) B_-\left(\omega' - q + k\right) B_+\left(-k + \frac{\Omega}{2}\right) dq + \text{conj.} \quad (\text{B25d})$$

$$+ \int_0^{\infty} B_-^*\left(\omega' - q - \frac{\Omega}{2}\right) B_+\left(\omega' - q - k\right) B_-\left(k + \frac{\Omega}{2}\right) dq + \text{conj.} \quad (\text{B25e})$$

$$+ \int_0^{\infty} dq \int_{-\infty}^{\infty} dq' B_+\left(q' - \frac{1}{2}\left(q - \omega' - \frac{\Omega}{2} + k\right)\right) B_-\left(-q' - \frac{1}{2}\left(k - \omega' - \frac{\Omega}{2} - k\right)\right) \quad (\text{B25f})$$

$$\times B_+^*\left(-q' - \frac{1}{2}\left(q - \omega' + \frac{\Omega}{2} + k\right)\right) B_-^*\left(q' - \frac{1}{2}\left(q - \omega' + \frac{\Omega}{2} - k\right)\right)$$

3. Numerical evaluation

a. Computation time

From a numerical point of view, the wavepacket propagator $K_{\text{wp}}(\omega, \omega'; \Omega)$ is easily evaluated since it only involves at most a single integral (the elastic scattering amplitude can be computed once and for all). Assuming an isotropic discretization with n points in both the ω and Ω directions, complexity of the wave packet contribution to single electron coherence then scales as $\mathcal{O}(n^3)$. The main computational difficulty arises from the term (B25f)

in the modified vacuum propagator $K_{\text{mv}}(\omega, \omega'; \Omega)$. This double integral has to be integrated twice, thus leading to a quadruple integral (complexity $\mathcal{O}(n^4)$). Introducing a discretization on the initial coherence with n^2 points, the full evaluation would naively lead to a $\mathcal{O}(n^6)$ complexity for the modified vacuum contribution to the outgoing coherence. It means that refining the discretization by a factor 2 would increase the computation time by a factor 64.

However, Eqs. (B12b) and (B12a) show that the problem has an intrinsic anisotropy: discretization in the ω variable should be adapted to take into account the en-

ergy scales introduced by the dynamics itself, whereas it is reasonable to think that discretization in the Ω direction should be determined by the time scales associated with the initial wavepacket. Therefore, introducing an anisotropic discretization with m points in the Ω direction and n points in the ω direction leads to an $\mathcal{O}(m \times n^5)$ complexity which is still very challenging.

Finally, Eq. (B23) can be used to decrease the complexity by one order of magnitude. At fixed, Ω , K_{mv} can be computed by decreasing ω and storing the integral of $\mathcal{F}_{\text{mv}}^{\text{(reg)}}$. Consequently only one evaluation of $\mathcal{F}_{\text{mv}}^{\text{(reg)}}$ is required and the total complexity can then be brought down to $\mathcal{O}(m \times n^4)$. Fortunately, the problem is well suited to parallelization: our C code exploits the OpenMP API interface and runs on a Dell PowerEdge R815 computer with 30 Opteron cores. Fig. 7 shows the scaling of the computing time as a function of the number of points n in the ω direction: a doubling $n \mapsto 2n$ leads to an increase by a factor ~ 15 , close to the expected $2^4 = 16$.

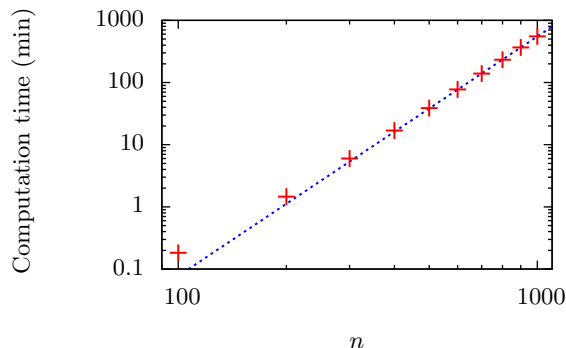


FIG. 7: Computation time as a function of the number n of points in the ω direction. Dashed curve is a linear fit in a log-log plot. Best fit is obtained with $t = \mathcal{O}(n^{3.85})$.

b. Testing the accuracy of the code

We have devised specific indicators to test the accuracy of the code: they are based on sum rules such as total charge conservation which had been used in our study of the relaxation of an electronic excitation with perfectly defined energy²⁵. In time dependent situations considered in the present paper, this sum rule is generalized into sum rules involving the time dependent average electric current.

More precisely, due to the relation between the Fourier components of the electrical current and the edge magnetoplasmon modes²¹, the average outgoing electric current can be computed straightforwardly from the incoming current and the edge magnetoplasmon transmission

amplitude $t(\omega)$:

$$\langle i(t) \rangle = -ev_F \int_{-\infty}^{+\infty} d\tau \chi(\tau) |\varphi_e(t - \tau)|^2 \quad (\text{B26a})$$

$$\chi(\tau) = \int_0^\infty (t(\omega)e^{-i\omega\tau} + \text{c.c.}) \frac{d\omega}{2\pi}. \quad (\text{B26b})$$

But it can also be computed directly from the excess Wigner function obtained by DFT from the excess single electron coherence in the frequency domain:

$$\langle i(t) \rangle = -e \int_{-\infty}^{+\infty} \Delta W_{\text{out}}^{(e)}(t, \omega) \frac{d\omega}{2\pi} \quad (\text{B27})$$

In practice, the case of a free propagation ($t(\omega) = e^{i\omega\tau}$) provides a stringent test of the code accuracy since increasing the time of flight τ introduces more and more oscillations in all the integrals that are evaluated. Free propagation is the worst situation for numerical convergence: in the case of an incoming Landau quasiparticle of duration τ_e and injected at energy $\hbar\omega_e$ such that $\omega_e\tau_e = 10$, the appearance of numerical errors can be seen on Fig. 8: at $\tau = 0.8\tau_e$, one clearly see that the computed outgoing excess Wigner function exhibits hole contributions which should not be present. The total charge departs from the expected value by 5 % for $\tau = 0.4\tau_e$ and by 45 % for $\tau = 0.8\tau_e$ and the electrical current (B27) computed from the excess Wigner function departs by 8 % from the expected one (B26a) for $\tau = 0.4\tau_e$ and by 25 % for $\tau = 0.8\tau_e$.

In the presence of interaction, the error rate is much lower since the integrals involved in the numerical computation do not involve purely oscillating functions. In order to avoid these problems and maximize the convergence speed of the numerics, we have also compensated for the global drift of the fractionalized current pulses by introducing a phase $e^{-i\omega\bar{\tau}}$ where $\bar{\tau} = (\tau_c + \tau_s)/2$ in front of the edge magnetoplasmon scattering matrix. Finally, the error rates corresponding to the interacting situations considered in the paper are much lower than the one discussed in the previous paragraph. Using parameters given in Table I, for Landau excitations at $\tau_s = \tau_e$, the total charge departs from the expected value by 1.8 % and the current by 6.3 %. For Levitov excitations at $\tau_s = 20\tau_0$, the total charge departs from the expected value by 4.9 % and the electrical current by 1.2 %.

c. Parameters choice

Table I summarizes the choice of parameters used to generate the results presented in the present paper. Discretization in the ω direction has been chosen to maximize accuracy of the results while keeping the computation time reasonable. This is challenging since a small discretization step in ω is required to ensure convergence of the numerical estimations of the integrals due to terms

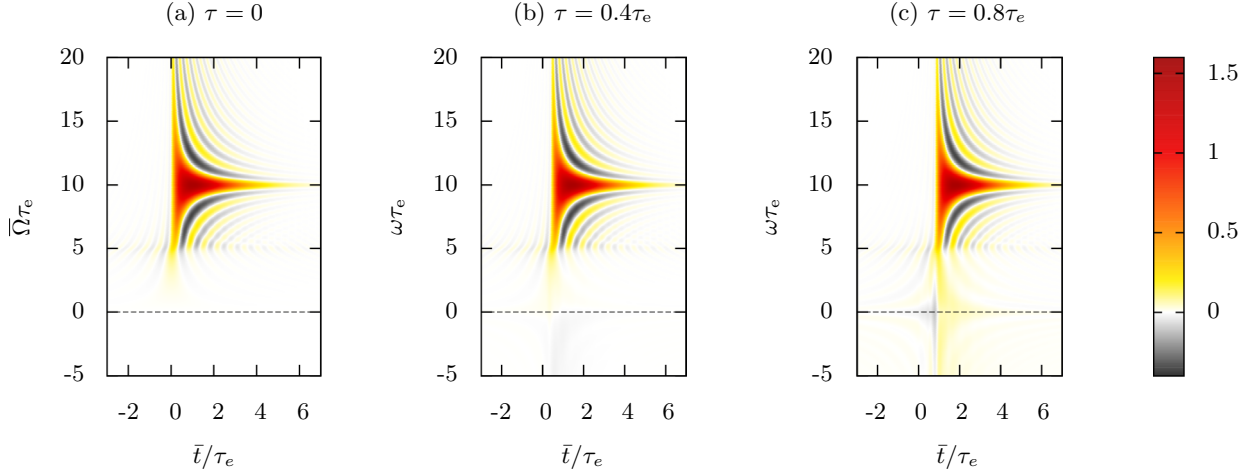


FIG. 8: Excess Wigner function $\Delta W^{(e)}(t, \omega)$ after free propagation for various time of flight τ : (a) incoming excitation with $\omega_e \tau_e = 10$, (b) outgoing excess Wigner function for $\tau = 0.4\tau_e$ and (c) for $\tau = 0.8\tau_e$. In the last case, numerical errors are clearly visible. These figures were obtained using a discretization with $n = 1024$ points in the ω direction and $m = 5 \times 1024$ in the Ω direction (time resolution 0.052 in t/τ_e).

Excitation	n	m	$\omega_{\max}/2\pi$	$\Omega_{\max}/2\pi$	δt
Landau	1024	5×1024	3	600	0.0052
Leviton	1024	5×1024	30	60	0.052

TABLE I: Parameters used to generate the figures presented in the paper for both the Landau and Leviton excitations. All parameters are given in units of the characteristic time scale of the excitation: τ_e for the Landau quasi-particle and τ_0 for the Leviton.

which oscillate faster with increasing copropagation distance. Moreover a sufficiently large interval for Ω is also needed so that the time dependence of the Wigner function over short time scales ($\lesssim \tau_e$ or $\lesssim \tau_0$) is captured.

The difference between the scales chosen between the Landau quasi-particle and the Leviton are justified by the expected scales of variations of the single electron coherence: in the frequency space, the Leviton coherence

is located close to the Fermi surface and decays exponentially ($\Delta \mathcal{G}^{(e)}(\omega + \Omega/2, \omega - \Omega/2)$ decays as $\exp(-2\omega\tau_0)$ for $\omega > 0$) whereas the Landau quasi-particle coherence decays algebraically. Consequently, we had to consider a much larger sampling domain for the coherence of Landau quasi-particles than for the Leviton.

Finally, videos have been generated to illustrate the evolution of the excess Wigner function for Landau and Leviton quasi-particles with increasing copropagation distances. Each of these videos involves 100 images.

Appendix C: Basic blocks for the case of $\nu = 2$

In the case of the $\nu = 2$ edge channel system, the auxiliary functions $B_{\pm}(\omega)$ can be computed analytically in closed form:

$$B_+(\omega) = -i\tau_c^{p_c} \tau_s^{p_s} \Theta(\omega) + \frac{p_s p_c}{2} + \frac{(\tau_s - \tau_c)^2}{\tau_c} e^{-i\omega\tau_c} \phi_1 \left[\frac{1}{2} + p_c, 1, 3; 1 - \frac{\tau_s}{\tau_c}, i\omega(\tau_s - \tau_c) \right] \quad (\text{C1a})$$

$$B_-(\omega) = \Theta(\omega) \left(i\tau_c {}_1F_1 [p_c, 1; i\omega(\tau_s - \tau_c)] + i(\tau_s - \tau_c) p_c {}_1F_1 \left[\frac{1}{2} + p_c, 2; -i\omega(\tau_s - \tau_c) \right] \right) \quad (\text{C1b})$$

where $p_{c/s} = (1 \pm \cos(\theta))/2$ and ${}_1F_1(\alpha, \beta; z)$ denotes the confluent hypergeometric function and $\phi_1(\alpha, \beta, \gamma; x, y)$ denotes the Humbert double series⁴¹. Finally, an analytical expression can also be obtained for the elastic scattering amplitude in term of the confluent hypergeo-

metric function ${}_1F_1$:

$$\mathcal{Z}(\omega_e) = e^{i\omega\tau_c} {}_1F_1 \left[\frac{1 + \cos(\theta)}{2}, 1; i\omega_e(\tau_s - \tau_c) \right]. \quad (\text{C2})$$

which reduces to a Bessel function at strong coupling. These analytical expressions have been used to check

the numerical solution of the integrodifferential equation (B16) with initial condition given by Eq. (B17).

-
- ¹ G. Fève *et al*, *Science* **316**, 1169 (2007).
² C. Leicht *et al*, *Semicond. Sci. Technol.* **26**, 055010 (2011).
³ J.D. Fletcher *et al*, *Phys. Rev. Lett.* **111**, 216807 (2013).
⁴ J. Dubois *et al*, *Nature* **502**, 659 (2013).
⁵ S. Hermelin *et al*, *Nature* **477**, 435 (2011).
⁶ S. Ol'khovskaya, J. Splettstoesser, M. Moskalets, and M. Büttiker, *Phys. Rev. Lett.* **101**, 166802 (2008).
⁷ E. Bocquillon *et al*, *Phys. Rev. Lett.* **108**, 196803 (2012).
⁸ E. Bocquillon *et al*, *Science* **339**, 1054 (2013).
⁹ C. Grenier *et al*, *Mod. Phys. Lett. B* **25**, 1053 (2011).
¹⁰ E. Bocquillon *et al*, *Annalen der Physik* **526**, 1 (2014).
¹¹ Y. Ji *et al*, *Nature* **422**, 415 (2003).
¹² P. Roulleau *et al*, *Phys. Rev. B* **76**, 161309 (2007).
¹³ I. Neder *et al*, *Nature Physics* **3**, 534 (2007).
¹⁴ P. Roulleau *et al*, *Phys. Rev. Lett.* **100**, 126802 (2008).
¹⁵ P.-A. Huynh *et al*, *Phys. Rev. Lett.* **108**, 256802 (2012).
¹⁶ C. Altimiras *et al*, *Nature Physics* **6**, 34 (2010).
¹⁷ H. Le Sueur *et al*, *Phys. Rev. Lett.* **105**, 056803 (2010).
¹⁸ L. Levitov, H. Lee, and G. Lesovik, *J. Math. Phys.* **37**, 4845 (1996).
¹⁹ E. Bocquillon *et al*, *Nature Comm.* **4**, 1839 (2013).
²⁰ I.P. Levkivskiy and E.V. Sukhorukov, *Phys. Rev. B* **78**, 045322 (2008).
²¹ C. Grenier *et al*, *Phys. Rev. B* **88**, 085302 (2013).
²² E. Berg *et al*, *Phys. Rev. Lett.* **102**, 236402 (2009).
²³ I. Neder, *Phys. Rev. Lett.* **108**, 186404 (2012).
²⁴ H. Kamata *et al*, *Nature Nanotechnology* **9**, 177 (2014).
²⁵ P. Degiovanni, C. Grenier and G. Fève, *Phys. Rev. B* **80**, 241307(R) (2009).
²⁶ D. Ferraro *et al*, *Phys. Rev. B* **88**, 205303 (2013).
²⁷ G. Haack, M. Moskalets and M. Büttiker, *Phys. Rev. B* **87**, 201302(R)(2012).
²⁸ I. Safi and H. Schulz, in *Quantum Transport in Semiconductor Submicron Structures*, 159 (Kluwer Academic Press, Dordrecht, 1995).
²⁹ I. Safi, *Eur. Phys. J. D* **12**, 451 (1999).
³⁰ P. Degiovanni *et al*, *Phys. Rev. B* **81**, 121302(R) (2010).
³¹ W.H. Zurek, S. Habib and J.P. Paz, *Phys. Rev. Lett.* **70**, 1187 (1993).
³² S. Deléglise *et al*, *Nature* **455**, 510 (2008).
³³ C. Altimiras *et al*, *Phys. Rev. Lett.* **105**, 226804 (2010).
³⁴ C. Neuenhahn and F. Marquardt, *Phys. Rev. Lett.* **102**, 046806 (2009).
³⁵ C. Wahl *et al*, *Phys. Rev. Lett.* **112**, 046802 (2014).
³⁶ T. Jonckheere, J. Rech, C. Wahl, and T. Martin, *Phys. Rev. B* **86**, 125425 (2012).
³⁷ J. Dubois *et al*, *Phys. Rev. B* **88**, 085301 (2013).
³⁸ C. Grenier *et al*, *New Journal of Physics* **13**, 093007 (2011).
³⁹ G. Haack, M. Moskalets, J. Splettstoesser and M. Büttiker, *Phys. Rev. B* **84**, 081303 (2011).
⁴⁰ H. Inoue, A. Grivnin, N. Ofek, I. Neder, M. Heiblum, V. Umansky, and D. Mahalu, preprint arXiv:1310.0691.
⁴¹ I. Gradshteyn and I. Ryzhik, *Table of integrals, series and products (fifth ed.)* (Academic Press, Inc, 1994).
⁴² Minimizing the partition noise³⁷ or controlling the harmonics of the drive ensures that undistorted Levitons arrive at the QPC.